DOI: 10.18154/RWTH-2025-04291

UnitCellSAED − An ImageJ-Based Tool for Determining Unit Cell Parameters from Selected Area Electron Diffraction Patterns

Thomas E. Weirich [1]

Gemeinschaftslabor für Elektronenmikroskopie (GFE), RWTH Aachen University,
Ahornstr. 55, D-52074 Aachen

30. April 2025

Abstract The macro program *UnitCellSAED* has been developed for the *ImageJ/Fiji* platform with the purpose of fast 2D unit cell parameter determination from zone axis SAED patterns. The program allows the user to impose different 2D symmetries (oblique, rectangular, square or hexagonal) on the determined 2D data sets for statistical testing. Aside from an error analysis by comparing observed and calculated d-spacings, the program calculates residuals and allows the re-indexing of the 2D HK indices to 3D hkl indices for subsequent use with other crystallographic software. The effectiveness of the developed code has been tested by the analysis of both synthetic and real SAED patterns. The results obtained from the analysis of simulated patterns prove that the code reliably and reproducibly calculates the lattice parameters. Furthermore, it is shown that the implemented algorithms and the measurement procedure do not introduce any systematic bias, so that the precision of the measurements is primarily limited by the uncertainty in the camera constant and, for real cases, by the quality of the obtained data.

1. Unit cell determination by selected area electron diffraction (SAED)

The determination of d-spacings and unit cell parameters by selected area electron diffraction (SAED) in a transmission electron microscope (TEM) is a standard method that is often employed for phase identification [Phillips 1960, Ferrel & Paulson 1977, Carr *et al.* 1989, Lyman & Carr 1992] or for characterisation of previously unknown compounds if the amount of the material is too small to perform XRD experiments [*e.g.* Weirich 2000]. In addition to materials identification, a precise monitoring of the variations in unit cell parameters can be of interest as it reveals internal stresses and structural transformations. Furthermore, a detailed knowledge of lattice parameters and lattice symmetry is an integral part of quality control in materials development. Another use of unit cell parameters from electron diffraction is for computational modelling of crystal structures by methods such as density functional theory [*e.g.* Albe & Weirich 2003, Weirich 2004].

In the past, several computer programs have been developed for the evaluation of SAED patterns. Some of these are *AUTO* [Brink & Tam 1996], *ELD* [Zou *et al.* 1993a, 1993b], *QED* [Belletti *et al.* 2000], *ProcessDiffraction* [Lábár 2005], *EXTRAX* [Dorcet *et al.* 2010], *DiffTools* [Mitchell 2008], *EDIFF* [Jiang *et al.* 2011], *autoSADP* [Wu *et al.* 2012], DIALS [Clabbers *et al.* 2018], *CrysTBox* [Klinger & Jäger 2015] and possibly a few other programs that not known by the present author. However, a considerable number of these programs prioritize intensity extraction for structural analysis rather than unit cell determination and are thus simply overloaded for the latter purpose. Another drawback is that many of these tools are not open source, which limits the users' ability to make modifications to meet their specific needs. Furthermore, several of these programs are bound to a specific operating system or are no longer maintained and therefore not available for newer versions of the operating system. These shortcomings and the need for an easy-to-use tool for the geometrical analysis of SAED patterns prompted the present author to develop the cross-platform ImageJ/Fiji macro application *UnitCellSAED.* The following describes the functionality of the developed code and reports on some benchmark tests that were performed to verify the correctness of the with *UnitCellSAED* obtained results.

[1] weirich@gfe.rwth-aachen.de

DOI: 10.18154/RWTH-2025-04291

2. Program description and general functionality

The macro code of *UnitCellSAED* was developed using the current freely available *FIJI* distribution of *ImageJ2* version 2.16.0/1.54p [Schindelin *et al.* 2012; Schneider *et al.* 2012]. As shown in the flowchart in Figure 1, the developed code is top-down with low modularisation. All formulas used in the program are listed in the mathematical appendix for reference.

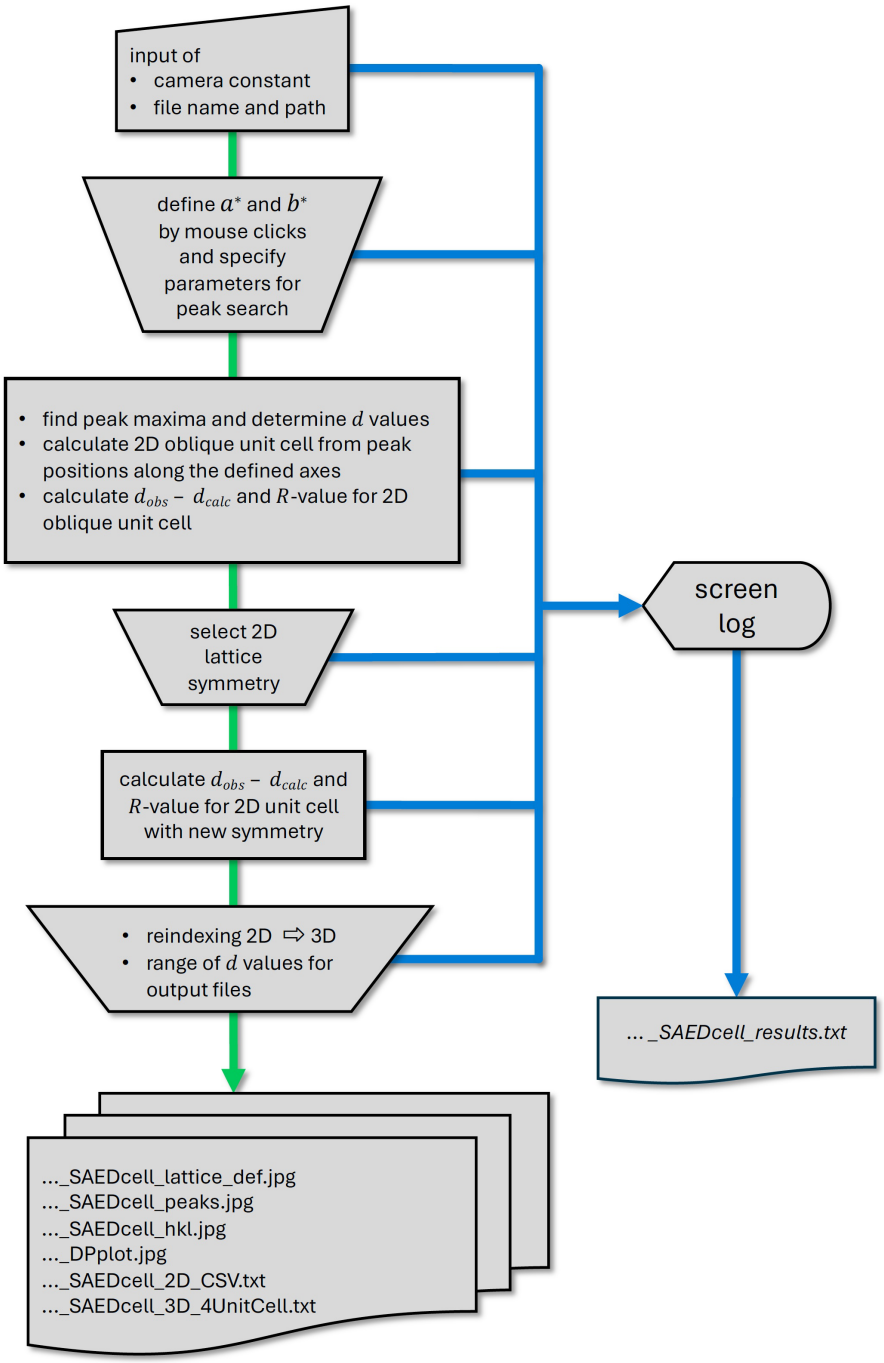

Figure 1. Flowchart of the *ImageJ* macro program *UnitCellSAED*.

After launch of the program the user is asked for the camera constant CC, the standard deviation σ_{CC} of the camera constant (both in Å·pixel units) and the filename and path of the SAED pattern to be to be analysed. The user is then requested to define the reciprocal A^* and B^* axes by clicking on two pairs of symmetry-related diffraction spots with the assigned lattice indices HO and -HO and OK and O-K, respectively. Each of these pairs of diffraction spots must be related by 2-fold symmetry, with the same distance of the diffraction spots from the centre of the pattern. After specifying the peak search radius around the estimated peak positions and defining a threshold for the peak detection, the program employs *ImageJ's* *FIND MAXIMA* function to determine the positions of the peak maxima of the diffraction spots within a by the user pre-defined resolution limit. Based on the peak positions on the defined reciprocal axes, the program calculates the two-dimensional real space 2D unit cell parameters a and b and the cell angle γ. The program allows the user to impose specific symmetries (oblique, rectangular, square or hexagonal) on the determined 2D lattice parameters and performs an error analysis by comparing the observed and calculated d-spacings to check the quality of the data set. Finally, the program allows the user to re-indexing and transform the 2D HK indices to 3D hkl indices for use with other software. As part of the analysis, the program generates several output files, including the full program log, files with the 2D HK or 3D hkl and d-spacings, and various images with overlays for reporting and documentation.

Output file name:	Content:
..._SAEDcell_lattice_def.jpg	Diffraction pattern with the marked peaks that have been selected by the user to define the 2D reciprocal lattice
..._SAEDcell_peaks.jpg	Diffraction pattern with markers for the detected peaks together with their 2D HK indices
..._SAEDcell_hkl.jpg	Diffraction pattern with markers for the detected peaks together with their 3D hkl Laue indices after reindexing
..._DPplot.jpg	Schematic diffraction pattern showing detected spots as circles with radius corresponding to peak intensity
..._SAEDcell_2D_CSV.txt	ASCII file with the HK indices and d-values of the 2D lattice (to be used for lattice refinement with the *UnitCell-2D* program [Weirich 2025]).
..._SAEDcell_3D_4UnitCell.txt	ASCII file with the hkl indices after reindexing and d-values (to be used for lattice refinement with the *UnitCell* program [Holland & Redfern 1997]).
..._SAEDcell_results.txt	ASCII file with complete screen log of the processing

3. Benchmarking

To check the performance of the code, three pseudo SAED patterns were generated using *JEMS* (https://www.jems-swiss.ch, version 4.13531u2024b31). The generated patterns are 832 × 832 pixels in size each and were calculated for a nominal camera length of L = 2500 mm with maximum possible excitation error, maximum acceptance radius and minimum angle of half convergence. A [001] simulated pattern for fcc gold (a = 4.0759 Å) was used to calibrate all patterns (CC = 179.08 ± 0.72 Å pixel). A post-statistical analysis of the calibration data suggests that the d-values, calculated with this camera constant, are ± 0.005 Å in error at maximum. The simulated patterns used for the benchmark tests were [001] fcc gold (a = 4.0759 Å, structure type *A1*), [001] cubic $SrTiO_3$ (a = 3.905 Å, structure type *E2₁*), and [001] hcp Mg (a = 3.209 Å, c = 5.211 Å, structure type *A3*).

DOI: 10.18154/RWTH-2025-04291

3.1. Results for [001] fcc gold

The primary objective of processing the simulated pattern of gold was to evaluate the reproducibility of the results, since the same pattern was used to determine the camera constant for the test patterns. For this pattern the peak search was carried with a threshold for *FIND MAXIMA* of 75 and 20 pixels around each estimated peak position (Figure 2). With these settings the program detected in total 56 peaks with a crystallographic resolution of 0.49 Å. The origin of the pattern was refined from 28 pairs of 2-fold symmetry related diffraction spots prior the calculation of the d-spacings and lattice parameters. The key results of this analysis are summarised in Table 1, together with the results of a subsequent least squares refinement with the d-values obtained from *UnitCellSAED*.

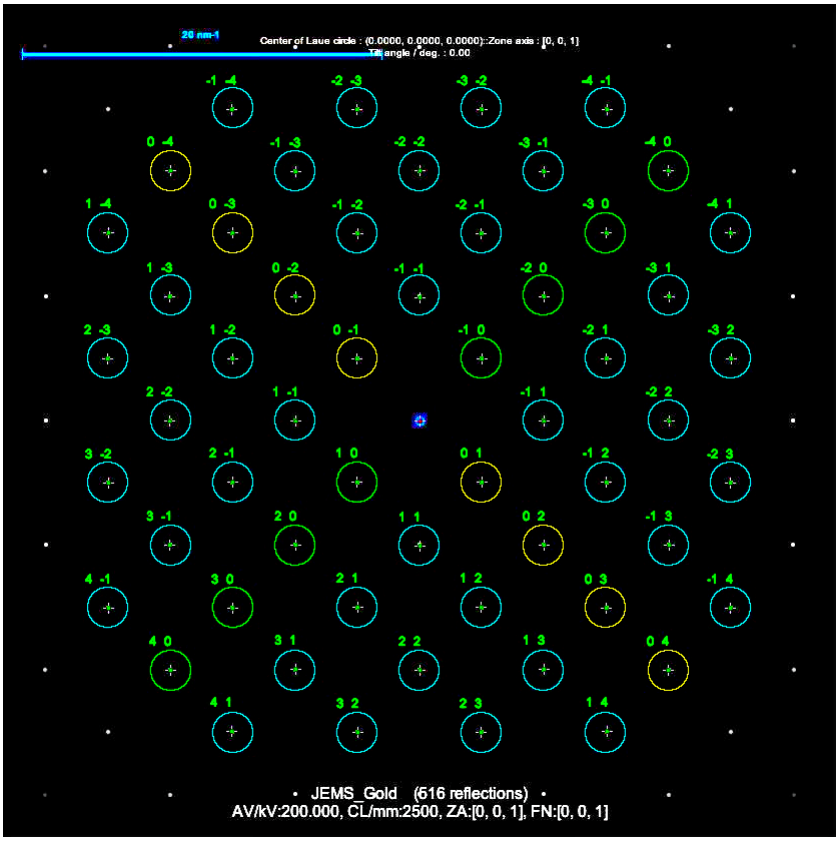

Figure 2.

Synthetic SAED pattern of [001] fcc gold from the *JEMS* simulation with circles that show the defined area for peak search. Areas that belong to the peak search along the A^* axis are indicated by green circles, while those along the B^* axis are marked by yellow circles. Peak positions found by the program are indicated by the green crosses.

Table 1. Key results from the processing of the [001] gold test pattern with *UnitCellSAED*.

Method	*N*	Sym.	a [Å]	b [Å]	γ [°]	$\sigma_{d,exp}$ [Å]	R_d-value [%]
calc. ma	16	oblique	2.0376	2.0376	90.31(22)	0.0042	0.30
LS	56	oblique	2.0353	2.0353	90.04	0.0041	0.27
calc. ma	16	square	2.0380		90	0.0038	0.25
LS	56	square	2.0353		90	0.0041	0.27

calc. ma: calculated from *N* diffraction spot positions along the user defined main axes
LS: least-squares refinement with *N* d-values using the program *UnitCell-2D* [Weirich 2025]
$\sigma_{d,exp}$: standard deviation of $d(obs) - d(calc)$

DOI: 10.18154/RWTH-2025-04291

A direct comparison of the two lattice parameters obtained for the 2D unit cell with square symmetry shows that the difference between the results is less than 0.003 Å, which is well within the calculated uncertainties (about 0.004 Å). Therefore, both results are considered as equivalent. Using these values, the lattice parameter for the 3D unit cell is obtained by multiplying the 2D lattice parameter by a factor of 2. This yields for the 2D square lattices before and after LS refinement values of a = 4.0760 Å and a = 4.0706 Å. These values for the lattice parameters differ from the value used for calibration by less than 0.0001 Å and 0.0053 Å, respectively. Surprisingly, the value determined here from the user-defined main axes is found much closer to the ideal lattice parameter of the calibration standard than that obtained from LS refinement with all data. Nevertheless, the close agreement between the uncertainty in the camera constant of σ_{CC} = 0.005 Å and for the LS refined 2D unit cell demonstrates that the former is the dominant factor determining the precision of the results, and that the implemented algorithm does not introduce any additional bias to the obtained data.

3.2. Results for [001] cubic strontium titanate $SrTiO_3$

This pattern was processed with the same parameters as in the previous case of fcc gold, *i.e.* a 20 pixels range around the estimated peak position and a *FIND MAXIMA* peak threshold of 75. Here the program detected in total 184 peaks up to 0.51 Å and the origin of the pattern was refined from 92 pairs of 2-fold symmetry related diffraction spots. The key results of this test run are summarised in Table 2.

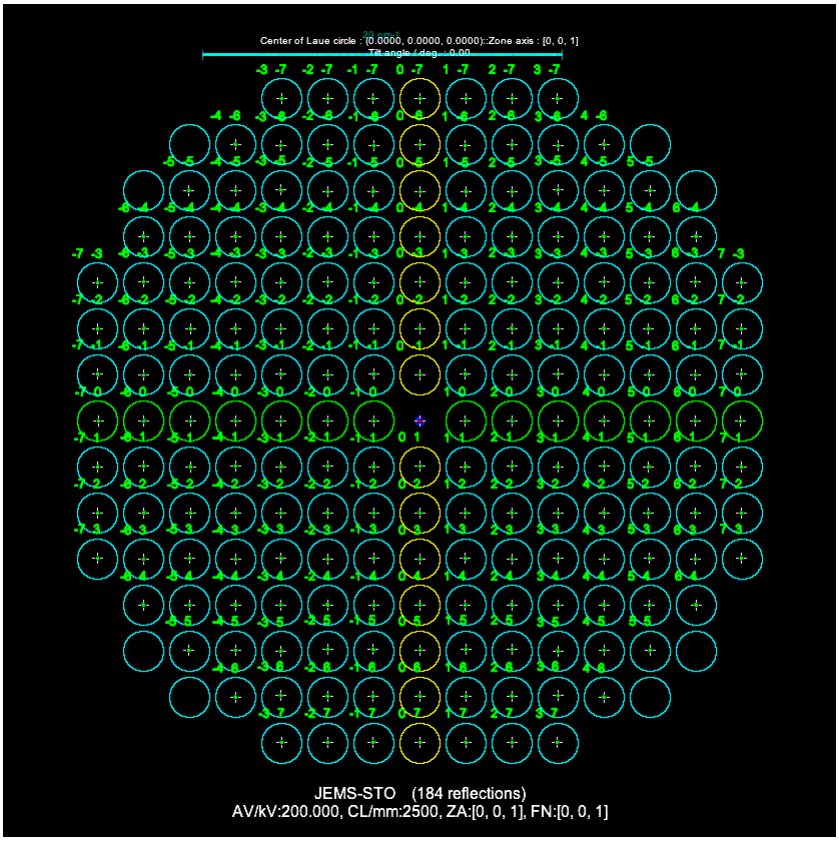

Figure 3.

Synthetic SAED pattern of [001] $SrTiO_3$ from the *JEMS* simulation with circles that show the defined area for peak search. Areas that belong to the peak search along the A^* axis are indicated by green circles, while those along the B^* axis are marked by yellow circles. Peak positions found by the program are indicated by the green crosses.

A direct comparison of the two lattice parameters obtained for the 2D unit cell with square symmetry shows that the difference between the two results is only 0.003 Å, which is less than half of the uncertainties of the measurement (about 0.007 Å, see Table 2). Again, both results are valid and statistically indistinguishable. The lattice parameters determined in this way for $SrTiO_3$ differ from the lattice parameter used in the *JEMS* simulation (a = 3.905 Å) by only 0.003 Å and

0.006 Å, which is within the determined experimental standard deviations. As for fcc gold in the previous test, the lattice parameter determined from the user-defined principal axes is again somewhat closer (but not statistically significant) to the reference lattice parameter used in the simulation than to the value obtained from least-squares refinement with the complete data set.

Table 2. Key results from the processing of the [001] $SrTiO_3$ test pattern with *UnitCellSAED.*

Method	*N*	Sym.	a [Å]	b [Å]	γ [°]	$\sigma_{d,exp}$ [Å]	R_d-value [%]
calc. ma	28	oblique	3.9032	3.9015	90.18(15)	0.0068	0.34
LS	184	oblique	3.8988	3.8990	90.0	0.0069	0.31
calc. ma	28	square	3.9020		90	0.0067	0.32
LS	184	square	3.8989		90	0.0069	0.31

calc. ma: calculated from *N* diffraction spot positions along the user defined main axes
LS: least-squares refinement with *N* d-values using the program *UnitCell-2D* [Weirich 2025]
$\sigma_{d,exp}$: standard deviation of $d(obs) - d(calc)$

3.3. Results for [001] hexagonal magnesium

The processing of this pattern, with a 15-pixel range around the estimated peak position and a peak threshold of 75, yielded 108 detected peaks, with 54 pairs of 2-fold symmetry-related diffraction spots that were used for calculating the pattern's origin. The main results of this analysis are summarised in the following Table (Table 3).

Table 3. Key results from the processing of the [001] pattern of hcp magnesium with *UnitCellSAED.*

Method	*N*	Sym.	a [Å]	b [Å]	γ [°]	$\sigma_{d,exp}$ [Å]	R_d-value [%]
calc. ma	20	oblique	3.2130	3.2130	120.21(30)	0.0050	0.37
LS	108	oblique	3.2031	3.2031	119.87	0.0053	0.28
calc. ma	20	hexagonal	3.2130		120	0.0050	0.39
LS	108	hexagonal	3.2052		120	0.0051	0.28

calc. ma: calculated from *N* diffraction spot positions along the user defined main axes
LS: least-squares refinement with *N* d-values using the program *UnitCell-2D* [Weirich 2025]
$\sigma_{d,exp}$: standard deviation of $d(obs) - d(calc)$

A direct comparison of the two lattice parameters obtained for the 2D unit cell with hexagonal symmetry shows a difference of about 0.008 Å, which exceeds the individual uncertainties of each result (about 0.005 Å). Nevertheless, both values differ from the lattice parameter used in the *JEMS* simulation for hcp magnesium (a = 3.209 Å) by only ± 0.004 Å, which is within the experimental standard deviation of 0.005 Å for both measurements. Hence, each result is a valid representation of the lattice in the processed diffraction pattern.

DOI: 10.18154/RWTH-2025-04291

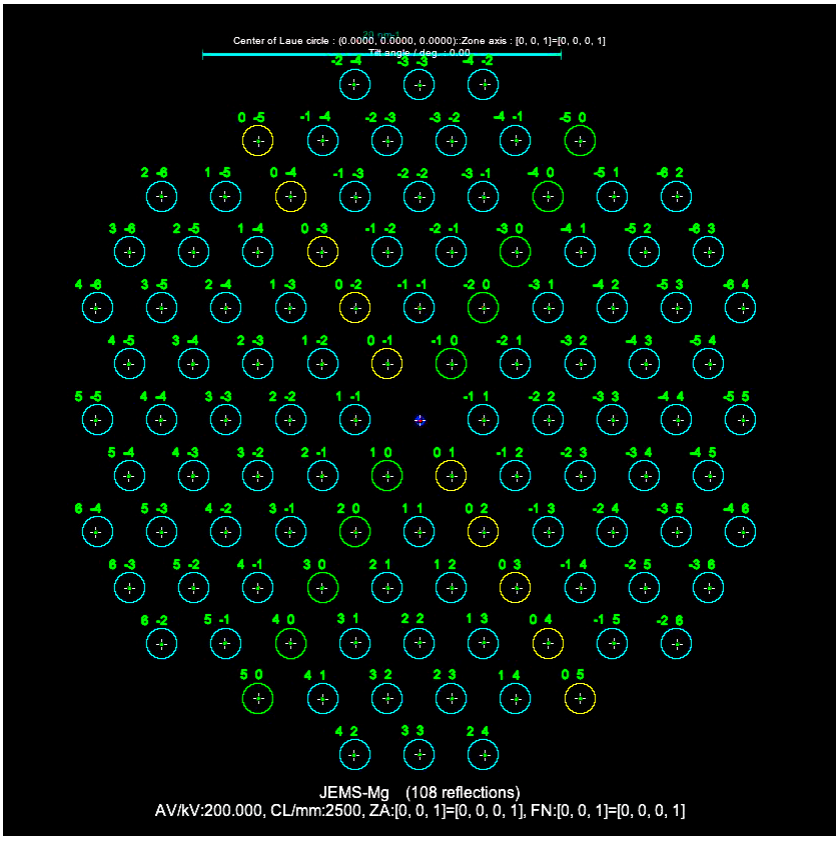

Figure 4.

Synthetic SAED pattern of [001] Mg from the *JEMS* simulation with circles that show the defined area for peak search. Areas that belong to the peak search along the A^* axis are indicated by green circles, while those along the B^* axis are marked by yellow circles. Peak positions found by the program are indicated by the green crosses.

3.4. Discussion of the benchmarking results

By processing three synthetic SAED patterns with *UnitCellSAED* it has been shown that the code provides reliable and reproducible lattice parameters from zone axis patterns with square and hexagonal symmetries. The lattice parameters calculated from only the peak positions along the defined main axes differ from the reference materials by a maximum of 0.004 Å. This value is in all cases equal to or less than the determined experimental standard deviations. Notably, in two of the three test cases the results based on the user defined principal axes were found slightly closer to the reference values than obtained from the LS refinements with all data. From a statistical point of view, however, these small differences are not significant. This shows that both methods can be used to determine lattice parameters, but the simpler principal axis approach using only the diffraction spots on the main axes may sometimes perform slightly better (at least in some cases for the synthetic SAED patterns analysed here). Furthermore, the analysis has shown that no systematic bias is introduced by the implemented algorithms nor by the measurement procedure, so that the precision of the results for ideal SAED patterns is primarily limited by the uncertainty σ_{CC} of the camera constant. The effect of the latter on the determined 2D lattice parameters can be estimated by the equation given in appendix 5.8, which is based on Gaussian error propagation. This gives estimated standard deviations of 0.0082 Å (Au), 0.0157 Å ($SrTiO_3$) and 0.0129 Å (Mg) for the here determined lattice parameters. This is an interesting point as these predicted values are at least twice as large as the standard deviations found in this study. Therefore, it can be concluded that the performance of the program likely exceeds the limits of the calibration, and that a more precise description for the camera constant will improve the precision of the determined lattice parameters.

Furthermore, the precision of the maximum determination is also affected by the *FIND MAXIMA* function of *ImageJ/Fiji*. A closer examination of the simulated diffraction pattern reveals that the diffraction spots for gold are characterised by a 4×4-pixel array with a varying intensity distribution. Additionally, slight variations in the distances between the peak centres can be observed. This

effect is however unavoidable when working with pixelated graphics. As the functionality of the *FIND MAXIMA* function itself is limited to full pixel values and a 4×4-pixel array cannot have a center pixel, the misplacement of the maximum is in the best case $\sqrt{2}/2$, *i.e.* 0.71 pixel. This misplacement has also a minor effect on the pattern center determination and therefore on the determined diffraction spot distances and the therefrom calculated d-spacings (see Table 4).

Table 4. Center positions *XY* of the test patterns determined by *UnitCellSAED.*

Test pattern	*XY* true pattern center	*XY* determined from *N* pairs of diffraction spots	*N*
fcc Au	416, 416	415.6, 415.7	28
cubic $SrTiO_3$	416, 416	415.7, 415.7	92
hcp Mg	416, 416	415.6, 415.9	54

If a peak misplacement of σ_R = 0.71 pixel is assumed as realistic, the estimated standard deviations for the lattice parameters will increase to 0.0184 Å for gold, 0.0624 Å for $SrTiO_3$ and 0.0429 Å for magnesium (CC = 179.08 ± 0.72 Å·pixel). Since the calculated *JEMS* SAED patterns mimic ideal conditions without electron-optical distortions, very sharply focussed diffraction spots with small half-widths, absence of alignment errors and an unbent and unstrained lattice, these estimated values for the precision are likely closer to the real measurement conditions, although the internal coherence of the data appears much better (see summary of results in Table 5).

Table 5. Experimental and calculated uncertainties σ_d with and without peak-detecting errors.

Test pattern	a [Å] Reference	a [Å] *UnitCellSAED*	$\sigma_{d,exp}$ [Å] *UnitCellSAED*	$\sigma_{d,cal}$ [Å] without peak misplacement	$\sigma_{d,cal}$ [Å] 0.71 pixel peak misplacement
fcc Au	$\frac{4.07593}{2}$	2.0380	0.0038	0.0082	0.0184
cubic $SrTiO_3$	3.905	3.9020	0.0067	0.0157	0.0624
hcp Mg	3.209	3.2130	0.0050	0.0129	0.0429

In this context, it should be noted that the expected precision can easily be improved by using a larger camera length according to the calculation formula. However, this approach also has its limits, as the larger the camera length, the fewer reflections can be recorded, which in turn leads to an increase in the inaccuracy of the determined d-values, as in any diffraction experiment [2].

[2] The error Δd for a d-spacing with distance R from the pattern center is given by $\Delta d = \left| CC \cdot \left[\frac{1}{R \pm \Delta R} - \frac{1}{R} \right] \right|$, where ΔR is the estimated measure error of a diffraction spot in pixel units.

4. Use cases

4.1. Ferritic high-silicon steel

The SAED pattern used in this example was obtained from a FIB cross section of a ferritic high-silicon steel examined at 200 kV in the FEI Tecnai F20 transmission electron microscope (TEM) in the authors' laboratory. The diffraction pattern was recorded along the bcc ⟨001⟩ direction at a nominal camera length of 970 mm using a Veleta 4-megapixel side-entry TEM camera from Emsis GmbH (Münster, Germany). Prior analysis with *UnitCellSAED*, a reference pattern of nanocrystalline gold was used to determine the camera constant and checked for elliptical distortion using another custom *ImageJ* script (CC = 446.45 ± 1.12 Å·pixel; elliptical distortion A/B = 1.006). No corrections were made to the diffraction pattern in this case as the elliptical distortion of the reference diffraction pattern is very small. The processing of the SAED pattern from the steel sample yielded 35 peak positions with d-values ranging from 2.0405 Å to 0.6312 Å. The oblique 2D unit cell, calculated from the diffraction spots along the user-defined axes, has the dimensions a = 2.0252 Å, b = 2.0129 Å, γ = 90.26(18)°. An error calculation based on this unit cell yielded a standard deviation of the d-value difference for all diffraction spots of 0.0043 Å with a residual R_d of 0.27 %. A subsequent least-squares refinement for the oblique cell with all 35 d-values from experiment gave a = 2.0194 Å, b = 2.0082 Å, γ = 90.11° with a standard deviation of the d-value differences of 0.0053 Å (R_d = 0.34 %.). A change in lattice symmetry from oblique to square gives an averaged lattice parameter a = 2.0190 Å with a cell angle of 90°. For this cell setting, the standard deviation of the d-value differences are 0.0053 Å with a residual R_d of 0.35 %. The subsequent least-squares refinement for the square cell gave a = 2.0140 Å, with a standard deviation σ_d of 0.0061 Å (R_d = 0.39 %). A summary of all results is found in Table 4.

Table 6. Key results from the processing of the ⟨001⟩ pattern of bcc iron with *UnitCellSAED.*

Method	*N*	Sym.	a [Å]	b [Å]	γ [°]	$\sigma_{d,exp}$ [Å]	R_d-value [%]
calc. ma	12	oblique	2.0252	2.0129	90.26(18)	0.0043	0.27
LS	35	oblique	2.0194	2.0082	90.11	0.0053	0.34
calc. ma	12	square	2.0190		90	0.0053	0.35
LS	35	square	2.0140		90	0.0061	0.39

calc. ma: calculated from *N* diffraction spot positions along the user defined main axes
LS: least-squares refinement with *N* d-values using the program *UnitCell-2D* [Weirich 2025]
$\sigma_{d,exp}$: standard deviation of $d(obs) - d(calc)$

Using the unrefined and LS-refined lattice parameters for the 2D square lattice allow to calculate the lattice parameter for bcc iron to a = 2.855 Å and a = 2.848 Å. A search for cubic structures with iron (Fe) and silicon (Si) in the International Centre for Diffraction Data (ICDD) PDF5+ database yielded a good match for the composition $Fe_{0.8}Si_{0.2}$ (PDF entry 04-003-3888, [Buschow *et al.* 1983]). In this case, the value obtained after LS refinement is closer to the value given in literature (a = 2.848 Å). Once again, a comparison of the experimental standard deviations shows that the calculated differences are not statistically relevant, since both results are within the range of uncertainty. Following the earlier outlined error propagation using CC = 446.45 ± 1.12 Å·pixel for the camera constant and an assumed peak misplacement of 0.71 pixel yields a = 2.848(15) Å as value for the lattice parameter of bcc iron in this sample.

DOI: 10.18154/RWTH-2025-04291

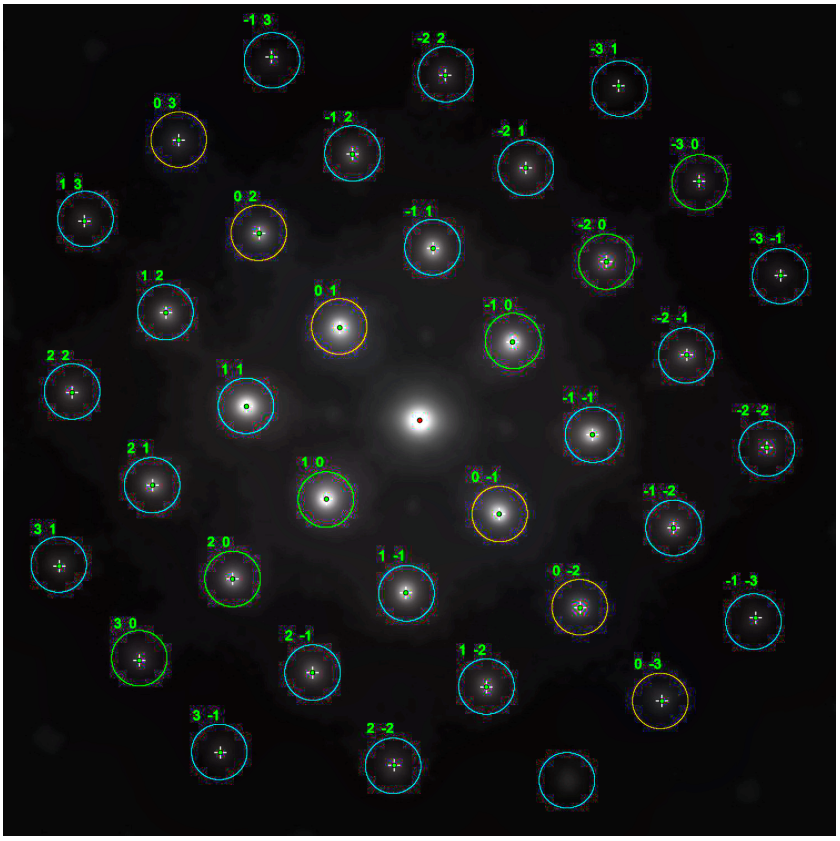

Figure 5.

SAED pattern of ⟨001⟩ bcc iron in high-silicon steel with circles that indicate the peak search area in the *UnitCellSAED* analysis. Areas corresponding to the peak search along the A^* axis are indicated by green circles, while those along the B^* axis are marked by yellow circles. The 35 peak positions found by the program are indicated by the green crosses.

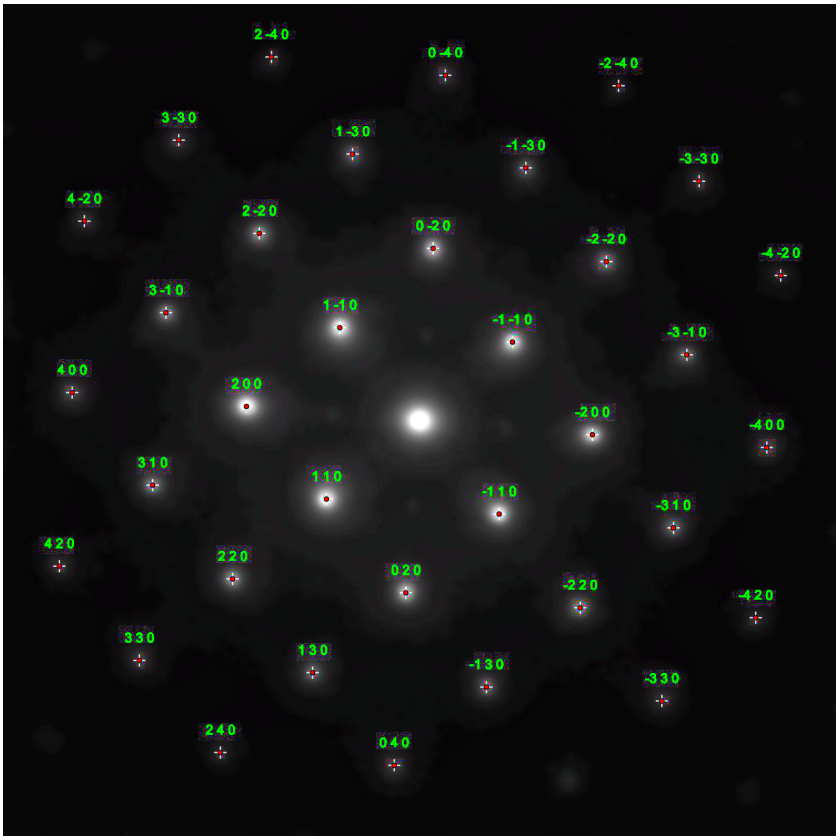

Figure 6.

SAED pattern of Figure 5 after reindexing the 2D indices with *UnitCellSAED* according to the true 3D bcc unit cell with zone axis orientation [001].

4.2. Molybdenum trioxide MoO_3

Small orthorhombic molybdenum trioxide crystals deposited on a carbon support film are a common test sample for calibrating the rotation angle between image and diffraction pattern [Fultz & Howe 2013]. The SAED pattern processed here was recorded along the [010] direction from such a test specimen (Plano GmbH, Wetzlar, Germany) using the FEI Tecnai F20 TEM at the authors' facility. All microscope settings were identical to those described in the previous section. The results from processing 98 HK data with d-values within 4.12 Å and 0.66 Å are summarized in Table 7.

Table 7. Results from processing the [010] pattern of orthorhombic MoO_3 with *UnitCellSAED.*

Method	*N*	Sym.	a [Å]	b [Å]	γ [°]	$\sigma_{d,exp}$ [Å]	R_d-value [%]
calc. ma	18	oblique	3.9552	3.6821	91.07(63)	0.0283	1.19
LS	98	oblique	3.9461	3.6712	90.28	0.0264	1.06
calc. ma	18	rectangular	3.9552	3.6821	90	0.0262	1.03
LS	98	rectangular	3.9472	3.6711	90	0.0265	1.06

calc. ma: calculated from *N* diffraction spot positions along the user defined main axes
LS: least-squares refinement with *N* d-values using the program *UnitCell-2D* [Weirich 2025]
$\sigma_{d,exp}$: standard deviation of $d(obs) - d(calc)$

Inspection of the differences between the observed and calculated d-spacings from the 2D lattice model shows that 21 (mostly) low order diffraction spots had a poor match with relative errors of up to 4%. Therefore, a second LS refinement was performed using only those reflections with less than 1% error in the first run. This resulted in a dataset of 77 HK data, yielding a refined oblique cell with a = 3.9414 Å, b = 3.6720 Å, γ = 90.30°. The corresponding uncertainty for the d-spacings is 0.0064 Å with a significantly lower R_d value of 0.53 %. The LS refinement for the rectangular 2D unit cell yields a = 3.9427 Å, b = 3.6718 Å with σ_d = 0.0068 Å and R_d = 0.54 %. Thus, the lattice parameters obtained here are well within the range of lattice parameters determined by XRD, *e.g.* a = 3.920 Å, c = 3.660 Å [Wooster 1931] and a = 3.9628 Å, c = 3.6964 Å [Kihlborg 1963]. Considering the errors introduced by the uncertainties of the camera constant σ_{CC} plus the assumed peak shift of 0.71 pixels, the lattice parameters determined directly by *UnitCellSAED* for the orthorhombic lattice are a = 3.9552 Å, c = 3.6821 Å with estimated uncertainties of 0.0268 Å and 0.0235 Å, respectively. It should be noted that these estimated uncertainties are very close to the experimentally determined standard deviation for this unit cell, before removing the low-resolution outliers from the data set. Thus it can be concluded that the here made assumptions about errors (σ_{CC}, peak shift) are close to physical reality.

DOI: 10.18154/RWTH-2025-04291

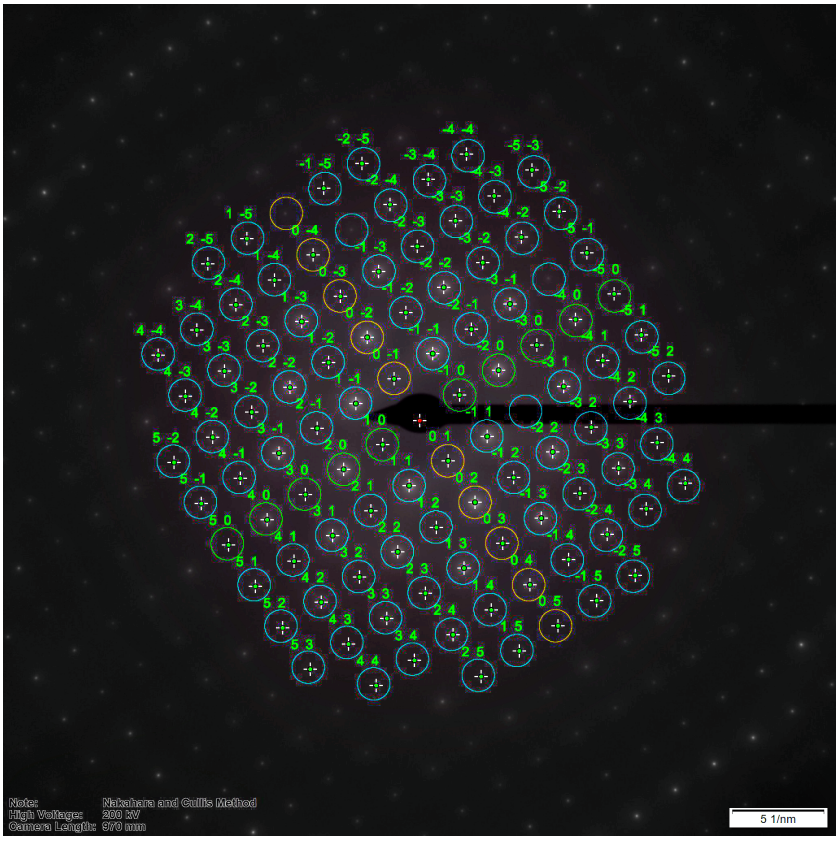

Figure 7.

SAED pattern of an orthorhombic MoO_3 platelet along the [010] zone axis with overlay from the analysis with *UnitCellSAED.*
The green crosses indicate the positions of the 98 detected peak positions with 19 peaks located along the by the user defined axes A^* (green) and B^* (yellow).

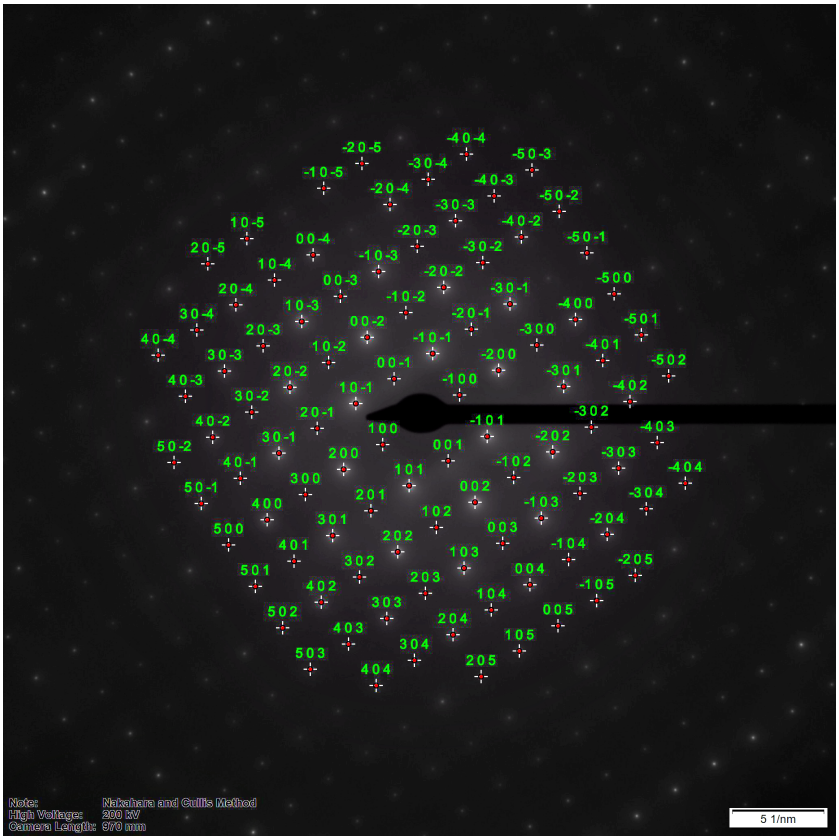

Figure 8.

SAED pattern of Figure 7 after reindexing the 2D indices with *UnitCellSAED* according to the true 3D unit cell with zone axis orientation [010].

DOI: 10.18154/RWTH-2025-04291

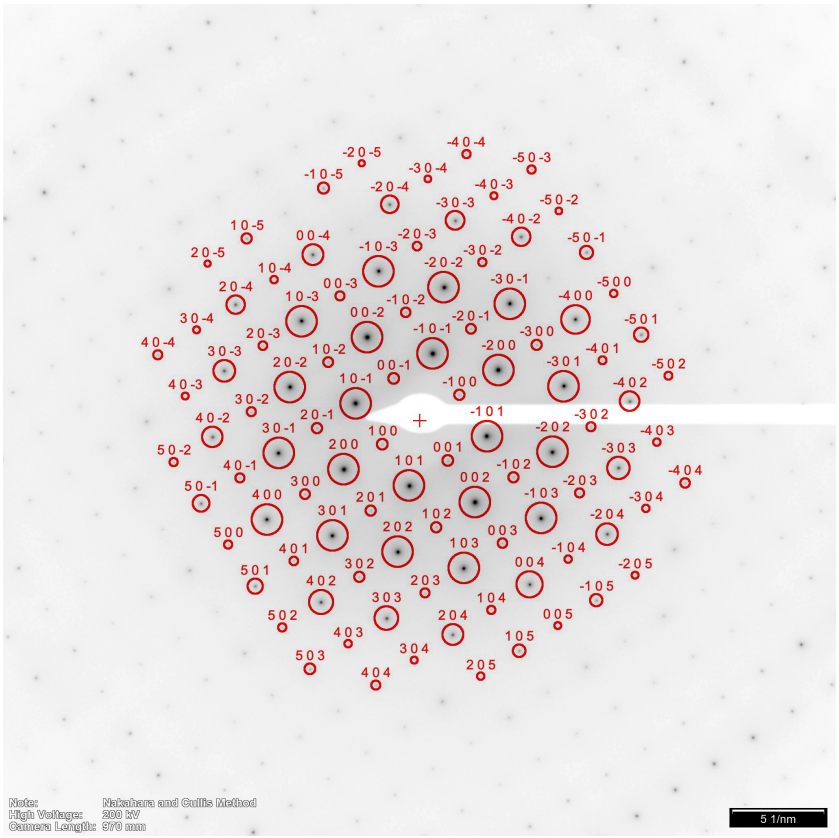

Figure 9.

Inverted SAED pattern of Figure 7 with the by *UnitCellSAED* generated overlay that shows circles whose radii are proportional to the detected peak intensities.

4.3. $Cs_xNb_{2.54}W_{2.46}O_{14}$

To evaluate the program's potential for analysing large unit cells, a SAED diffraction pattern of the complex oxide $Cs_xNb_{2.54}W_{2.46}O_{14}$, recorded during an earlier investigation on film [Weirich *et al.* 2006], was analysed. The in Figure 10 shown [001] SAED pattern of the compound was recorded on Kodak SO-163 sheet film using the FEI Tecnai F20 TEM at the authors facility and then digitised at 600 dpi with a flatbed scanner, yielding an image of 1464 × 1984 pixels in size. Prior to the analysis with the program *UnitCellSAED*, the central region was cut out and digitally enlarged to 300 %. Processing of the enlarged SAED pattern with CC = 1713.74 Å·pixel and a peak threshold of 100 yielded 334 peak positions with d-values above 2 Å (Figure 11). The oblique 2D unit cell, retrieved from the d-values of the principal axes gave a = 27.7961 Å., b = 21.6060 Å, γ = 90.75(60)° with σ_d = 0.6584 Å and R_d of 3.48 %. A change in lattice symmetry from oblique to rectangular using the same values for the lattice parameters yielded σ_d = 0.6570 Å with R_d = 3.23 %. The slightly better results for the rectangular 2D lattice suggest that the latter likely represents the true lattice symmetry. However, as can be seen in Figure 11, the program has detected some peaks in the central region of the primary beam, which were also part of this evaluation. As these peaks are clearly artefacts, they should be excluded from the calculation of the lattice constants. Therefore, before exporting the d-values for the final LS refinements, an upper limit for the d-spacings at 7 Å was defined that excludes these unwanted reflections. The applied limit, represented by the blue circle in Figure 11, reduced the number of the available d-spacings for the LS refinements by just 10 values. A least-squares refinement for the oblique cell with this new data set of 324 d-spacings gives a = 27.1947 Å, b = 21.6202 Å, γ = 90.20° with a standard deviation of the d-value differences of 0.0786 Å (R_d = 1.73 %). A corresponding LS refinement for a rectangular cell yielded a = 27.1967 Å, b = 21.6203 Å, with a standard deviation σ_d of 0.0786 Å (R_d = 1.74 %). For comparison all results are summarized in Table 4.

DOI: 10.18154/RWTH-2025-04291

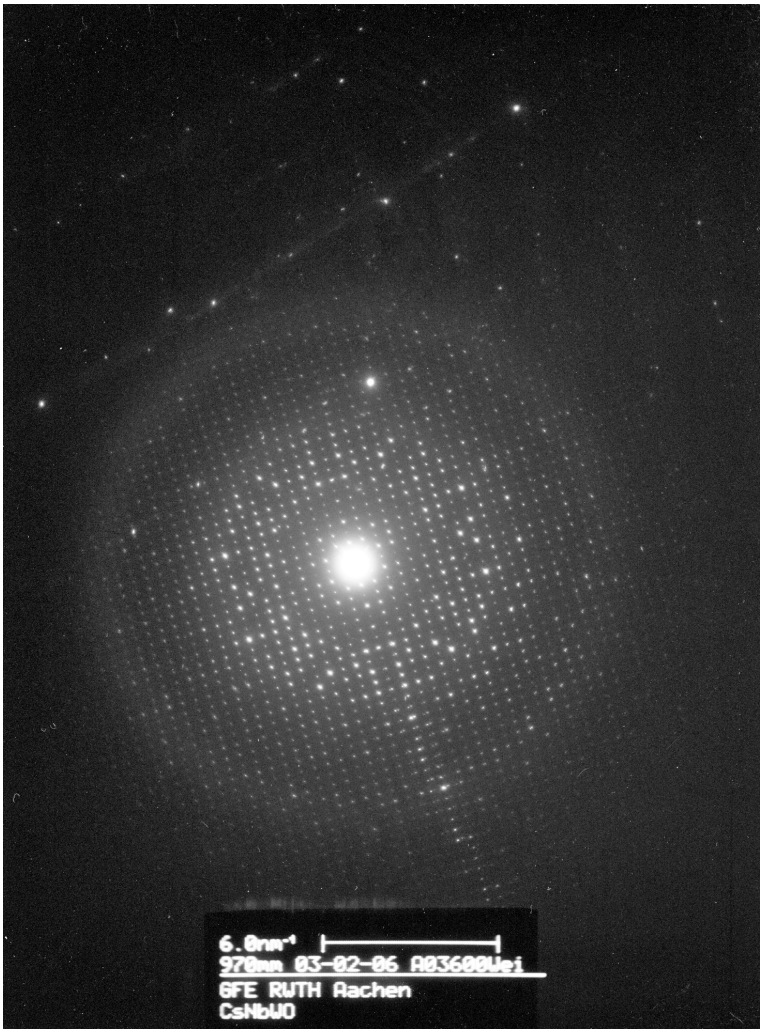

Figure 10.

SAED pattern of a $Cs_xNb_{2.54}W_{2.46}O_{14}$ crystal along the [001] zone-axis. The SAED pattern was initially recorded on Kodak SO-163 sheet film using the FEI Tecnai F20 TEM at the authors' facility and then digitised with a flatbed scanner at 600 dpi, yielding an image of 1464Å×1984 pixels in size. Prior to the analysis with the program *UnitCellSAED*, the central region was cut out and digitally enlarged to 300%.

Table 8. Results from the processing of the [001] pattern of $Cs_xNb_{2.54}W_{2.46}O_{14}$ with *UnitCellSAED.* The reference values for orthorhombic $Cs_xNb_{2.54}W_{2.46}O_{14}$ as determined from Rietveld refinement are a = 27.145(2) Å, b = 21.603(2) Å [Weirich et al. 2006].

Method	*N*	Sym.	a [Å]	b [Å]	γ [°]	$\sigma_{d,exp}$ [Å]	R_d-value [%]
calc. ma (all)	22	oblique	27.7961	21.6060	90.75(60)	0.6584	3.48
LS (max. 7 Å)	324	oblique	27.1947	21.6202	90.20	0.0786	1.73
calc. ma (all)	22	rectangular	27.7961	21.6060	90	0.6570	3.23
LS (max. 7 Å)	324	rectangular	27.1967	21.6203	90	0.0786	1.74

calc. ma: calculated from *N* diffraction spot positions along the user defined main axes
LS: least-squares refinement with *N* d-values using the program *UnitCell-2D* [Weirich 2025]
$\sigma_{d,exp}$: standard deviation of $d(obs) - d(calc)$

As can be seen from the results in Table 8, ignoring the d-spacings larger than 7 Å in the LS refinements had a significant impact, as it led to a reduction of the R values by about a factor of 2 and improved the standard deviations by about one order of magnitude. This result is not unexpected, since the error in determining the d-spacings increases as the distance to the centre

DOI: 10.18154/RWTH-2025-04291

decreases (see footnote on p. 9). However, the determined experimental standard uncertainty for the LS refined 2D unit cell is quite large and many of the observed d-spacings differ by a few percent from their calculated value (see Figure 12). A closer inspection of the fine structure of the diffraction spots showed that many of the reflections are asymmetric in shape and intensity distribution. Whether this asymmetry is related to a misalignment of the TEM (*e.g.* a not fully corrected condenser system) or to the quality of the crystal (stacking faults, internal stresses) is difficult to resolve almost two decades after the investigation. However, that the used SAED pattern is not ideal can be seen in Figure 10, which shows another overlapping [001] Laue circle in the lower right part and several additional diffraction spots that not belong to the regular lattice of the crystal under investigation. To check the regularity of the reciprocal lattice and thus the quality of the crystal the distances between the diffraction spots were calculated and visualised (see Figure 13). This analysis shows that many spot-to-spot distances are consistent with the ideal values from LS refinement, but there are also several pairs of diffraction spots that show significant deviations from these values. As the deviations appear to be random rather than systematic, they are more likely to be related to a poorly defined or defect-rich crystal lattice than to other sources of error. However, despite the non-optimal data set with resolution only up to d_{min} = 2 Å, the lattice parameters derived from it are remarkably close to those previously determined by Rietveld refinement on the same sample (see Table 8), *i.e.* 27.197 Å *vs.* 27.145 Å for the a-axis and 21.620 Å *vs.* 21.603 Å for the b-axis. These differences correspond to relative deviations of only 0.19% and 0.08% respectively.

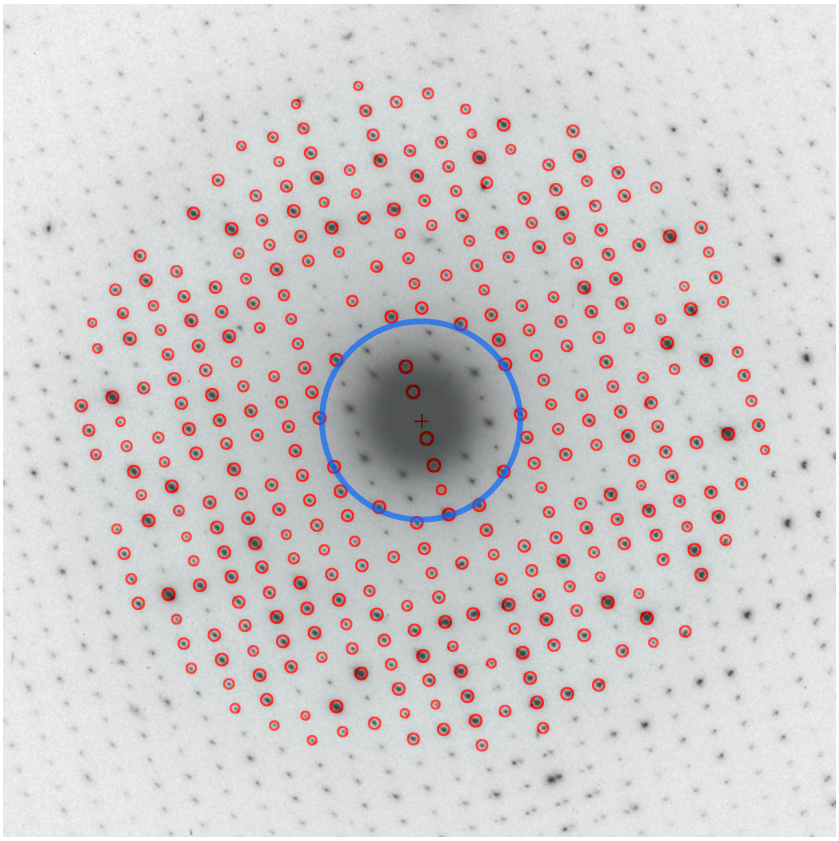

Figure 11.

Magnified central part of the inverted SAED pattern shown in Figure 10. The blue ring marks the 7 Å upper limit used to exclude the inner reflections from the LS refinement of the 2D unit cell. LS refinement using the 324 d-values from the encircled diffraction spots outside the blue ring with a resolution of up to 2 Å gives a = 27.197 Å, b = 21.620 Å for the rectangular 2D unit cell ($\sigma_{d,exp}$= 0.079 Å, R_d = 1.74 %).

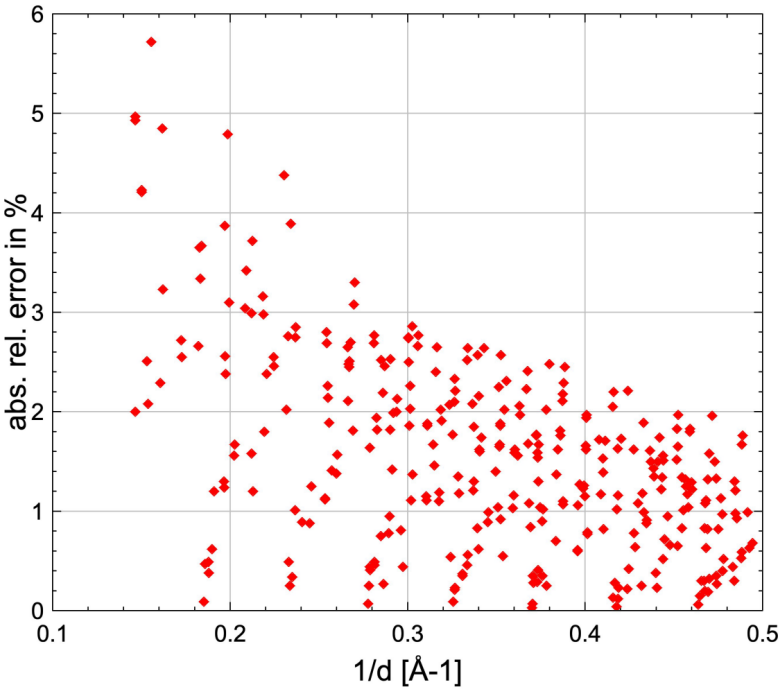

Figure 12.

Plot of the relative errors $\frac{|d_{obs}-d_{cal}|}{d_{obs}}$ after least-squares refinement of the rectangular 2D unit cell with 324 d_{obs} values between 7 and 2 Å. Aside the typical trend that the measure error decreases with increasing distance of a spot from the pattern center, the large scatter of the errors indicates that the quality of the data is not very high.

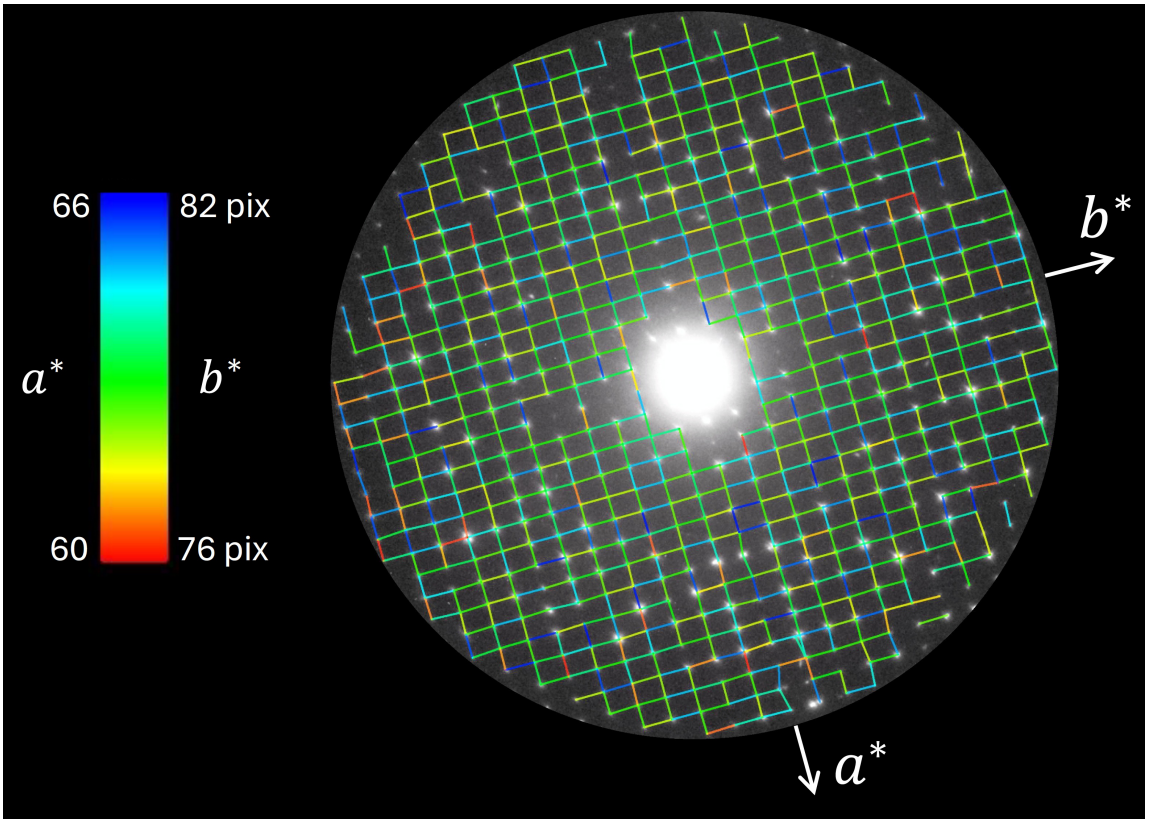

Figure 13. Regularity check of the reciprocal lattice for the SAED pattern in Figure 10. The lattice parameters for the a- and b-axes from the LS refinement correspond to 63- and 79-pixel direct spot-to-spot distances in the diffraction pattern. The visualisation shows the colour coded distances along the two main axes with a variation of ± 3 pixels around each LS refined value. This interval corresponds to a range of 26.0 Å to 28.6 Å or 4 % to 5 % error for the a-axis and 20.9 Å to 22.5 Å or 3 % to 4 % error for the b-axis. In addition to the many diffraction spots that have distances close to the refined lattice parameters (green lines), there are also several pairs of diffraction spots that show significant higher and lower values. As the deviations appear to be random rather than systematic, they are more likely to be related to a poor-defined or defect-rich crystal lattice than to other sources of error.

Acknowledgements

The experimental diffraction patterns of ferrite and MoO_3 used in this report were recorded and kindly provided by Ms Jacqueline Gehlmann and Mr Jonas Werner (GFE, RWTH Aachen University).

References

Albe, K., Weirich, T.E. (2003). Acta Cryst. A, 59, 18-21. DOI: 10.1107/S0108767302018275

Andrews, K. W., Dyson, D. J. & Keown, S. R. (1968). Interpretation of Electron Diffraction Patterns, 2nd ed. London: Adam Hilger.

Belletti, D., Calestani, G., Gemmi, M., & Migliori, A. (2000). Ultramicroscopy, 81(2), 57–65. DOI: 10.1016/S0304-3991(99)00118-7

Brink, J., & Tam, M. W. (1996). Journal of Structural Biology, 116(1), 144–149. DOI: 10.1006/jsbi.1996.0023

Buschow, K.H.J., Van Engen ,P.G., Jongebreur, R. (1983). J. Magn. Magn. Mater. 1983, 38, 1. DOI: 10.1016/0304-8853(83)90097-5

Carr, M.J., Chambers, W.F., Melgaard, D., Himes, V.L., Stalick, J.K., Mighell, A.D. (1989). Journal of Research of the National Institute of Standards and Technology 94(1), 15–20. DOI: /10.6028/jres.094.003

Clabbers, M. T. B., Gruene, T., Parkhurst, J. M., Abrahams, J. P., & Waterman, D. G. (2018). Acta Cryst. D, 74, 506–518. DOI: 10.1107/S2059798318007726

Dorcet, V., Larose, X., Fermin, C., Bissey, M. and Boullay, P. (2010). J. Appl. Cryst., 43, 191–195. DOI: 10.1107/S0021889809049267

Ferrell Jr., R.E., Paulson G.G. (1977). Micron, 8(1-2), 47–55. DOI: 10.1016/0047-7206(77)90009-7

Fultz, B., Howe, J. (2013). Transmission Electron Microscopy and Diffractometry of Materials, 4th edn., Springer-Verlag Berlin Heidelberg, sec. A.12.1, p. 723–725. DOI: 10.1007/978-3-642-29761-8

Holland, T. J. B., Redfern, S. A. T. (1997). J. Appl. Cryst., 30 (1), 84. DOI: 10.1107/S0021889896011673.

Jiang, L., Georgieva, D. and Abrahams, J.P. (2011). J. Appl. Cryst., 44, 1132–1136. DOI: 10.1107/S0021889811030731

Klinger, M., & Jäger, A. (2015). J. Appl. Cryst. 48, 2012–2018. DOI: 10.1107/S1600576715017252

Kihlborg, L. (1963). Arkiv for Kemi, 21, 357–364.

Laue, M. (1948). Materiewellen und ihre Interferenzen, 2nd Edn., Akademische Verlagsgesellschaft Geest & Portig K.G., Leipzig, p. 136.

Lábár, J.L. (2005). Ultramicroscopy, 103, 237–249. DOI: 0.1016/j.ultramic.2004.12.004

Lyman, C.E., Carr, M. J. (1992). In: Electron Diffraction Techniques, Vol.2, Cowley, J.M. (ed.), Oxford University Press, Chapter 5 (Identification of Unknowns), 373–17. DOI: 10.1093/oso/9780198555582.003.0005

Mitchell, D.R.G. (2022). Microsc Res Tech., 85, 2708–2713. DOI: 10.1002/jemt.24124

Mitchell, D.R.G. (2008). Microsc. Res. Tech., 71: 588–593. DOI: 10.1002/jemt.20591

Phillips R. (1960). Br. J. Appl. Phys. 11 504–506. DOI: 10.1088/0508-3443/11/11/305

Reimer, L. (1993). Transmission Electron Microscopy - Physics of Image Formation and Microanalysis, Springer-Verlag Berlin Heidelberg 1993. DOI: 10.1007/978-3-662-21556-2

Schindelin, J., Arganda-Carreras, I., Frise, E. et al. (2012). Nature Methods **9**, 676–682. DOI: 10.1038/nmeth.2019

Schneider, C. A., Rasband, W. S., & Eliceiri, K. W. (2012). Nature Methods, 9(7), 671–675. DOI: 10.1038/nmeth.2089

Weirich, T.E. (2000). Acta Cryst A, 56, 29–35. DOI: 10.1107/s0108767399009605.

Weirich, T.E. (2004). Acta Cryst. A, 60, 75–81. DOI: 10.1107/S0108767303025042

Weirich, T. E., Portillo, J., Cox, G., Hibst, H., Nicolopoulos, S. (2006). Ultramicroscopy, 106(3), 164–175. DOI:.org/10.1016/j.ultramic.2005.07.002

Weirich, T.E. (2025). *UnitCell-2D*: A JavaScript program for the determination and refinement of two-dimensional unit cell parameters from indexed d-spacings using the least-squares method (unpublished).

Wooster, N. (1931). Z. Kristallogr., 80, 504. (ICDD PDF# 01-075-0912)

Wu, C. H., Reynolds, W. T., Jr, & Murayama, M. (2012). Ultramicroscopy, 112(1), 10–14. DOI: 10.1016/j.ultramic.2011.09.013

Zou, X.D., Sukharev, Y., Hovmöller, S. (1993a). Ultramicroscopy, 49, 147–158. DOI: 10.1016/0304-3991(93)90221-I

Zou, X.D., Sukharev, Y., Hovmöller, S. (1993b). Ultramicroscopy, 52, 436–444. DOI: 10.1016/0304-3991(93)90058-6

DOI: 10.18154/RWTH-2025-04291

5. APPENDIX

5.1. Calculation of experimental d-spacings

The calculation of the experimental d-spacings is carried out with the standard formula *) for evaluating electron diffraction patterns [Andrews *et al.* 1968].

$$d_{HK} = \frac{CC}{R_{HK}}$$

d_{HK} d-spacing (d-value, interplanar distance) of diffraction spot HK
CC camera constant (obtained from a ring pattern using $CC = d_{hkl} \cdot R_{hkl}$)
R_{HK} distance of diffraction spot HK from the pattern center

---

*) The above equation has been derived for small electron wavelengths using the small-angle approximation [Ferrell & Paulson 1977]. However, careful measurement of the camera constant at medium-high accelerations of about 100 kV and below has shown that the camera constant decreases slightly with increasing distance of a diffraction spot from the pattern centre [Phillips 1960]. To correct this, an additional term can be added to the evaluation formula [Andrews *et al.* 1968], in which the factor $3/8$ accounts for the difference between $\tan 2\vartheta$ and $\sin \vartheta$ [Laue 1948, Reimer 1993].

$$R \cdot d_{hkl} = CC \cdot \left(1 + \frac{3R^2}{8L^2}\right)$$

If the virtual camera length L is replaced by CC/λ, an expression is obtained that easily allows to calculate the error in d if the geometrical correction is not applied.

$$d_{hkl} = \frac{CC}{R} + \frac{3}{8} \cdot \frac{R \cdot \lambda^2}{CC}$$

Thus at 200 kV ($\lambda = 0.025079$ Å) and a camera constant of 180 Å·pixel this equation yields without the correction for 360 pixel a d-value of 0.5 Å. Using the geometrically corrected equation gives a d-spacing of 0.5005 Å, which is only 0.1% larger than the former and thus negligible in the sense of other errors that can be 10 times larger, such as an often-present elliptical distortion of the pattern [Mitchell 2022].

5.2. Calculation of the average d-spacings for the main axes

The average d-spacing ($H = 1, K = 0$) of the a axis is calculated from:

$$\bar{d}_a = \frac{\sum_i (\, d_i \cdot |H_i| \,)}{N_a}$$

d_i d-spacing of diffraction spot i with Laue indices $H_i \neq 0$ and $K = 0$
N_a Number of used reflections with Laue indices $H \neq 0$ and $K = 0$
$\bar{d}_a$ average d-spacing corresponding to the a axis ($H = 1, K = 0$)

The calculation of the average d-spacing for the b axis ($H = 0, K = 1$) is carried out in analogy.

5.3. Calculation of the mean angle γ^* between the main axes

The reciprocal angle γ^* between the reciprocal axes A^* and B^* is directly calculated from the positions of the diffraction spots in the pattern. The distance and direction of each diffraction spot from the pattern center is represented by a vector. For each combination of the vectors $\vec{A}$ and $\vec{B}$ the angle between them can be calculated from:

$$\gamma^*_{AB} = \cos^{-1}\frac{\vec{A}\cdot\vec{B}}{|\vec{A}|\cdot|\vec{B}|}$$

The mean angle γ^* between the principal reciprocal axes is the average calculated from the sum of N angles $\gamma^*_{AB,i}$:

$$\gamma^* = \frac{\sum_i \gamma^*_{AB,i}}{N}$$

5.4. Calculation of the lattice parameters of the 2D unit cell

The real space lattice parameters for the main axes a and b and the angle γ of the 2D unit cell are calculated from:

$$a = \frac{\bar{d}_a}{\sin\gamma^*}$$

$$b = \frac{\bar{d}_b}{\sin\gamma^*}$$

$$\gamma = 180° - \gamma^*$$

5.5. Calculation of d-spacings from 2D lattice parameters

The d-spacings of the calculated 2D unit cell can be obtained from:

$$\frac{1}{d_{hk}} = \frac{1}{\sin\gamma}\sqrt{\frac{h^2}{a^2}+\frac{k^2}{b^2}-\frac{2hk}{ab}\cos\gamma} = \sqrt{h^2a^{*2}+k^2b^{*2}+2hka^*b^*\cos\gamma^*}$$

where

$$a^* = \frac{1}{a\cdot\sin\gamma}$$

$$b^* = \frac{1}{b\cdot\sin\gamma}$$

5.6. Calculation of the standard deviation for $d_{obs} - d_{cal}$

The standard deviation $\sigma_{d,exp}$ of N differences between the experimental determined d-spacings d_{obs} and the corresponding d-spacings d_{cal} , calculated from the determined 2D unit cell, is given by

$$\sigma_{d,exp} = \sqrt{\frac{1}{N-1} \cdot \sum_{i=1}^{N} \left(d_{obs,i} - d_{cal,i} - \overline{d_{obs} - d_{cal}}\right)^2}$$

Herein is $\overline{d_{obs} - d_{cal}}$ the average difference of the d-spacings calculated from

$$\overline{d_{obs} - d_{cal}} = \frac{\sum_{i=1}^{N} \left(d_{obs,i} - d_{cal,i}\right)}{N}$$

5.7. Calculation of the residual R_d

The residual (R-value) for the determined 2D unit cell is calculated from.

$$R_d = \frac{\sum |d_{obs} - d_{cal}|}{\sum d_{obs}}$$

5.8. Estimate of the standard deviation of the determined 2D lattice parameters

If only the error of the determined camera constant on the d-values and the uncertaincy of the determined diffraction spot positions is considered Gaussian error propagation yields the following estimate for the standard deviation σ_d of a determined d-value:

$$\sigma_{d,cal} = \sqrt{\left(\frac{d \cdot \sigma_{CC}}{CC}\right)^2 + \left(\frac{d^2 \cdot \sigma_R}{CC}\right)^2}$$

Herin is σ_{CC} the standard deviation of the camera constant CC and σ_R is an assumed error for determining the diffraction spot position on the detector. In the current version of *UnitCellSAED* (version 1.6en) the lattice parameters and a and b are used instead of the d-value to estimate their standard deviation. The error for determining the diffraction spot position is by standard assumed as zero (σ_R = 0) in this estimate.